CONTRAST MEDIA & MOLECULAR IMAGING

Received: 20 November 2015, Revised: 20 May 2016, Accepted: 27 May 2016, Published online in Wiley Online Library: 4 July 2016

(wileyonlinelibrary.com) DOI: 10.1002/cmmi.1704

Design of functionalized gold nanoparticle probes for computed tomography imaging

Alessandro Silvestri[a,b†], Vanessa Zambelli[c†], Anna M. Ferretti[a], Domenico Salerno[c], Giacomo Bellani[c]* and Laura Polito[a]*

The development of new molecules able to efficiently act as long-circulating computed tomography (CT) contrast agents is one of the most crucial topics in the biomedical field. In the last years, the chance to manipulate materials at the nano-size level gave new boost to this research, with the specific aim to design innovative nanoprobes. Gold nanoparticles (AuNPs) have showed unique X-rays attenuation properties which, combined with their easy surface functionalization, makes them ideal candidates for the next generation of contrast agents. In this paper, we present a rational and facile approach to synthesize engineered and water-stable AuNPs, achieving concentrated colloidal solution with high Hounsfield Units (HU). An accurate control of reagents ratio allowed us to design AuNPs with different shapes, from symmetrical to anisotropic morphology, in a convenient 'one-pot' fashion. Their activity as efficient and reliable CT contrast agents has been evaluated and compared. Moreover, glucosamine-functionalized gold nanoparticles have been developed ([Au] = 31.20 mg/mL; HU = 2453), in order to obtain a CT contrast agent able to combine spatial resolution with metabolic information. Copyright © 2016 John Wiley & Sons, Ltd.
Additional supporting information may be found in the online version of this article at the publisher's web site.

Keywords: gold nanoparticles; X-ray contrast agents; surface modifications; micro-CT

1. INTRODUCTION

Computed tomography (CT) is a widespread non-invasive medical imaging technique, characterized by good resolution, high efficiency and low cost (1,2). In contrast with other techniques, such as Positron Emission Tomography (PET), CT scan has a lower sensitivity and lack of the ability to track specific metabolic pathways (e.g., glucose metabolism). In some instances, due to the lack of natural contrast from tissues, it can be necessary to provide contrast with exogenous agents, to acquire more detailed information about the regions of interest. Nowadays, the most widespread CT contrast agents are hydrophilic polyiodinated compounds, characterized by a quick renal clearance and a good vascular permeability (3). Nevertheless, these agents carry drawbacks in clinical use, primarily related to renal toxicity, allergic reactions and other side effects (4). Even if these limitations are rare events, in the last years efforts have been devoted to the development of new CT contrast agents based on nano-materials (5,6). The possibility of manipulating nano-sized materials tuning their features, makes nanotechnology an exciting field of development for 'smart' contrast agents able to circulate for prolonged period in the blood pool and to actively target a specific site. Among the candidates as next generation CT contrast agents, gold nanoparticles play a crucial role, thanks to their easy surface functionalization, high X-ray absorption coefficient and good biocompatibility. To date, various gold nanostructures have been synthesized and tested as potential CT contrast agents, pointing out the high potentiality of this material (7–14). Some of the most important features for well-tolerable contrast agents are their easy elimination by the body, their prolonged circulation in the blood, and the lack of toxicity. In this context, some papers reported the synthesis of ultrasmall **AuNPs**, able to be cleared through renal excretion, hence avoiding the detrimental accumulation of the metal in organs (13,14). Moreover, in the attempt to use the minimal amount of contrast agents, great efforts have been devoted to surface functionalization, exploiting an active targeting to the site of interest. Gold nanoparticles, in fact, can be stably engineered at the surface, taking advantage of the strong soft-soft interaction between sulfur and gold atoms. By exploiting this chemistry, it is possible to load on the vast and available surface area several active compounds, which can help the selectivity of the contrast agents or even act as therapeutics. Besides and before clinical use, these kinds of nanomaterials can act as effective and powerful pre-clinical contrast nano-agents. For these reasons, continuous improvements on reliable

* *Correspondence to: L. Polito, CNR – ISTM, Nanotechnology Lab., Via G. Fantoli 16/15, 20138 Milan, Italy; and G. Bellani, Department of Medicine and Surgery, University of Milano-Bicocca, Via Cadore 48, 20900 Monza, Italy. E-mail: laura.polito@istm.cnr.it; giacomo.bellani1@unimib.it*

† *These authors contributed equally to the article.*

a *A. Silvestri, A. M. Ferretti, L. Polito*
CNR – ISTM, Nanotechnology Lab., Via G. Fantoli 16/15, 20138, Milan, Italy

b *A. Silvestri*
Department of Chemistry, University of Milan, Via C. Golgi 19, 20133, Milan, Italy

c *V. Zambelli, D. Salerno, G. Bellani*
Department of Medicine and Surgery, University of Milano-Bicocca, Via Cadore 48, 20900, Monza, Italy

synthesis and biological evaluation of surface-coated **AuNPs** are necessary.

Here, we report the synthesis of highly stable and functionalized gold nanoparticles with the aim of elucidating the main factors involved in their *in vivo* bio-distribution. To achieve this result, the surface coatings and the morphologies of the core have been fine tuned. By modifying described procedures, gold nanoparticles have been synthesized through a 'one-pot' methodology which allowed us to obtain functionalized symmetrical or anisotropic nanoparticles by means of an accurate modulation of the reagents ratio. Anisotropic nanoparticles, as star-shaped gold nanoparticles, are emerging as innovative nanomaterials since they can be exploited as multimodal contrast agents for CT imaging and surface enhanced Raman spectroscopy (SERS) (15,16). Considering the great interest towards anisotropic nanoparticles features (17), we were particularly interested in a deeper evaluation of their *in vivo* properties as CT contrast agents, depending on the dimension and in a comparison with symmetric shaped nanoparticles. Heterobifunctional thiolated polyethylene glycols (HS-PEG_{5000}-COOH and HS-PEG_{5000}-OMe) have been evaluated as biocompatible polymers (18) to stabilize gold colloidal solutions and to increase their circulation time in blood pool. Then, taking advantage of the available carboxylic group of HS-PEG_{5000}-COOH, we developed a proof-of-principle glucosamide-coated nano-tracer characterized by an active targeting towards glucose uptake, and hence metabolic activity. It is commonly known, in fact, that neoplastic and inflammatory cells show enhanced dependence from the glycolitic pathway, (also in aerobic conditions), resulting in an increased cellular uptake of glucose (19,20). For this reason the metabolism of 2-deoxy-D-glucose is still extensively studied (21) and its analogue 2-([^{18}F]fluoro)-2-deoxy-D-glucose (2FDG) is widely used as radiotracer in PET-CT, for the detection of tumours and inflammatory sites (22,23). All functionalized **AuNPs** were subjected to a full characterization by Transmission Electron Microscopy (TEM), Inductively Coupled Plasma-Optical Emission Spectrometers (ICP-OES), UV–vis spectroscopy and Dynamic Light Scattering (DLS). The structural information obtained were correlated with the results of the *in vivo* experiments, conducted by means of micro-CT imaging, to evaluate PEGylated **AuNPs** activity as X-ray contrast agents and the time course of their systemic distribution.

2. RESULTS AND DISCUSSION

2.1. Synthesis and characterization of functionalized gold nanoparticles

Up to date, a vast number of protocols to synthesize gold nanoparticles are available in literature (24). Nevertheless, the identification and development of improved strategies for synthesizing **AuNPs** is an extremely important and crucial step, tightly linked with their final application, surface functionalization and colloidal stability. Among the large pool of existing procedures to produce **AuNPs** in aqueous environment (24,25), Turkevich protocol (26) is the most common and flexible one and a number of revised methods are reported (27). For example, in 2011 Schütz *et al*. reported a seed mediated procedure based on Turkevich methodology to prepare water-stable gold anisotropic nanoparticles (28). By modifying the protocol described in this paper, we developed a 'one-pot' strategy to obtain functionalized **AuNPs** with different core morphologies (Fig. 1), using sodium citrate and hydroquinone as reducing agents. This protocol allowed us to control the anisotropy of the core without the addition of toxic templating agents such as cetyl trimethylammonium bromide (CTAB). Moreover, the procedure can afford the synthesis of a large quantity of functionalized **AuNPs**, without the need to purify the intermediate citrate-stabilized nanoparticles. The selected ligands, in fact, were added directly to the mixture, to stop and cap nanoparticles' growing. The general protocol required the seeds synthesis by adding gold salts, pre-incubated with sodium citrate and silver nitrate, to boiling water. The seeds formation is almost immediate, but to ensure the complete reduction and enhance the crystal uniformity, the reaction mixture was stirred for 45 min at 100 °C before starting the growing step.

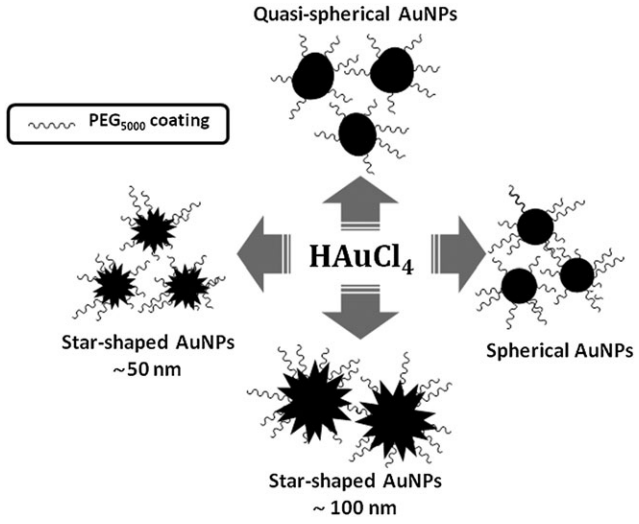

Figure 1. Schematic representation of the synthesized **AuNPs**, obtained by means of reductive reaction of $HAuCl_4$ and stabilized with different types of polyethylene glycol (PEG). Dimensions for star-shaped **AuNPs** are referred to the core size.

A pre-activated mixture of $HAuCl_4$, $AgNO_3$ and sodium citrate was added to the cooled seeds mixture, followed immediately by a solution of hydroquinone in order to grow the seeds. The colloidal mixture was stirred at room temperature for 1 hour before capping the nanoparticles by means of thiolated polyethylene glycols addition. For our purpose, HS-PEG_{5000}-COOH, HS-PEG_{5000}-OMe and HS-PEG_{5000}-CONHGlucose [see **Supporting Information** (**SI**)] were screened as ligands. A PEG coating guaranteed the indispensable colloidal stability and imparted to nanoparticles the stealth towards macrophages, therefore a prolonged blood circulation (29). The purified engineered **AuNPs** can be concentrated at small volume (few hundreds of microliters) resulting in samples characterized by a high concentration of gold, which still maintain stability up to months of storage. Noteworthy, this aspect is essential owing to the high amount of gold necessary for setting each *in vivo* experiment. By an accurate modulation of the relative amount of the reagents, we were able to produce 'one-pot' quasi-spherical (**AuNP2-AuNP4**), spherical (**AuNP6**, **AuNP7**) or anisotropic (**AuNP9**) functionalized gold nanoparticles (Scheme 1 and Table 1).

AuNP2 and **AuNP4**, characterized by a quasi-spherical shape, were synthesized as described (see Experimental part and **SI**, Fig. 8 and 10 respectively), changing the capping ligand in the final step of the synthesis (HS-PEG_{5000}-COOH for **AuNP2** and

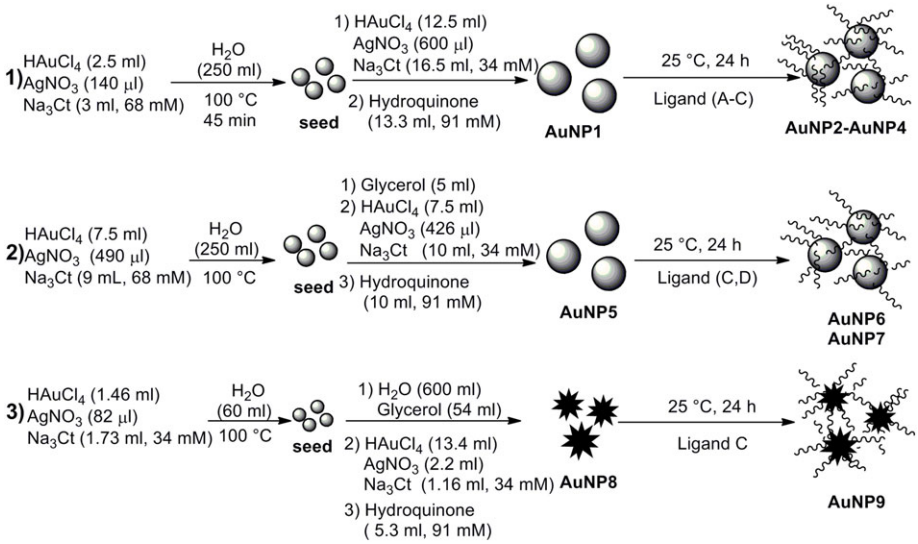

Scheme 1. Synthesis of **AuNP 1–9**. $[HAuCl_4] = 10$ mM; $[AgNO_3] = 5.9$ mM; PEG ligands: **A**: HS-PEG_{5000}COOH (**AuNP2**); **B**: HS-PEG_{5000}COOH/HS-PEG_{5000}OMe 1/1 (**AuNP3**); **C**: HS-PEG_{5000}OMe (**AuNP4**, **AuNP6**, **AuNP9**); **D**: HS-PEG_{5000}CONHGlucose (**AuNP7**). Abbreviations: Na_3Ct = sodium citrate.

Table 1. Description of engineered **AuNPs**, summarizing morphology, coating, hydrodynamic diameter (D_H), Zeta-potential (ζ-potential), gold concentration and X-rays attenuation of the solutions

Samples	*Morphology*	*Coating*	*D_H (nm)*	*ζ-potential (mV)*	*[Au] mg/ml*	*HU in vitro*
AuNP2	Quasi-spherical	HS-PEG_{5000}-COOH	27.04	−37.64	35.00	3378
AuNP3	Quasi-spherical	HS-PEG_{5000}-COOH/ HS-PEG_{5000}-OMe	39.03	−29.76	28.12	2304
AuNP4	Quasi-spherical	HS-PEG_{5000}-OMe	40.87	−23.00	28.75	2376
AuNP6	Spherical	HS-PEG_{5000}-OMe	39.82	−20.00	23.01	2062
AuNP7	Spherical	HS-PEG_{5000}-CONHGlucose	33.51	−21.00	31.20	2453
AuNP9	Star	HS-PEG_{5000}-OMe	52.69	−18.79	22.04	1834
AuNP11	Star	HS-PEG_{5000}-OMe	176.30	−17.54	7.67	424

HS- PEG_{5000}-OMe for **AuNP4**). The crystal structure corresponding to Au metal is confirmed by the Electron Diffraction (ED) (SI, Fig. 12). An improved control over dispersion and shape was obtained by adjusting the reagents ratio and adding glycerol in the growing step of the synthesis (28,30), affording spherical samples **AuNP6** (coated by HS-PEG_{5000}-OMe) and **AuNP7** (coated by HS- PEG_{5000}-CONHGlucose). **AuNP6** (Fig. 2A) is characterized by a median diameter of 15.8 nm ± 3.1 nm, while **AuNP7** (Fig. 6) by a median diameter of 16.6 nm ± 3.9 nm. Totally anisotropic **AuNP9** (Fig. 2B), characterized by the presence of urchins and functionalized by HS-PEG_{5000}-OMe (Scheme 1 and Table 1), have been easily synthesized modulating the ratio of the reagents during the second step of growth.

To evaluate the effect of the size for urchinated **AuNPs**, we synthesized 'one-pot' functionalized gold nanostars by exploiting the use of hydroquinone as unique reducing agent, following a procedure reported in literature (31), yielding **AuNPs** characterized by an enhanced core dimension (**AuNP11**, Table 1, SI Fig. 11). Finally, gold nanoparticles were purified and fully characterized in terms of morphology, composition, coating functionalization and X-rays absorption (Table 1).

In Table 1, the ability of the colloidal gold solutions to absorb X-rays is reported as Hounsfield Units (HU) measured *in vitro* by micro-CT scan. The linear correlation between HU and gold concentration suggests that X-rays absorption is not affected by core morphology, size or surface coatings (see **SI**, Fig. 13).

2.2. *In vivo* CT imaging of functionalized gold nanoparticles

Micro-CT imaging in live healthy mice were performed to evaluate the biodistribution of **AuNPs**. Following intravenous administration of gold nanoparticles, mice remained alive for at least four hours from the injection and in most cases (**AuNP 4-6-9-11**) up to 24 hours (sacrifice). We measured the X-rays attenuation in the liver and in the blood pool within the heart, to evaluate stealthness and prolonged persistence in the blood of engineered **AuNPs**, comparing the behavior of the different nanostructures (Fig. 3 and Fig. 4). Even if each nano-system showed a high colloidal stability and an efficient X-rays absorption, we identified **AuNP6** and **AuNP9** as the most promising to act as efficient and safe CT contrast agents. It can be noticed that **AuNPs** displaying carboxylic acids on their surface (**AuNP2** and **AuNP3**) were quickly internalized in the liver, and after 1 hour from injection of these **NPs**, mice displayed a high contrast in the liver. In the same way, the nano-system characterized by the highest hydrodynamic diameter (**AuNP11**) led to an important increase of liver contrast, despite the lack of residual free charges on their surface.

These results can be better visualized in Fig. 4, which summarizes the temporal trend of HU, expressed as heart/liver ratio, over the time of observation. On the basis of the present results, we do show that metal core anisotropy does not play any

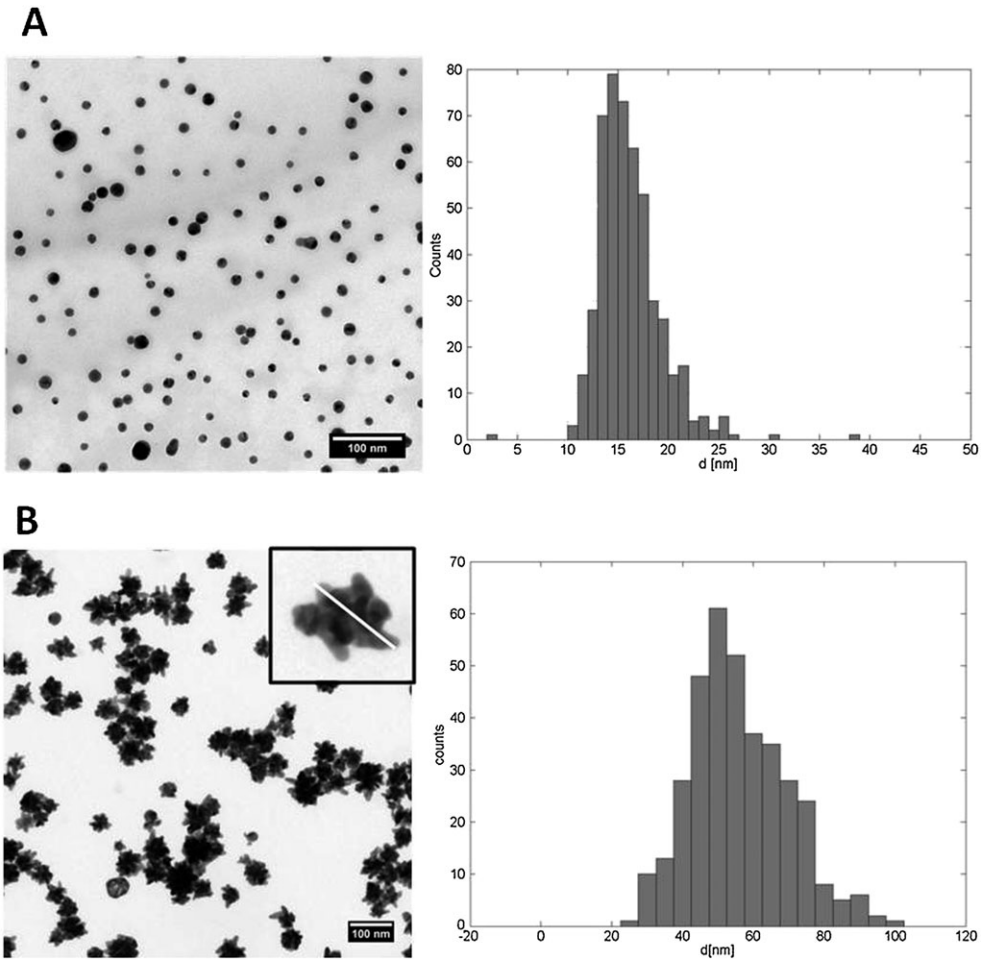

Figure 2. **A**. Left: TEM micrograph of **AuNP6** sample. Right: statistical distribution of particles diameters: $d_{median} = 15.8 \pm 3.1$ nm; **B**. Left: TEM micrograph of **AuNP9** sample. Right: statistical distribution of branch length (inset of TEM micrograph) having minimum value 27.0 nm and maximum value 100.9 nm. The median value was 54.2 nm (standard deviation of 13.6 nm).

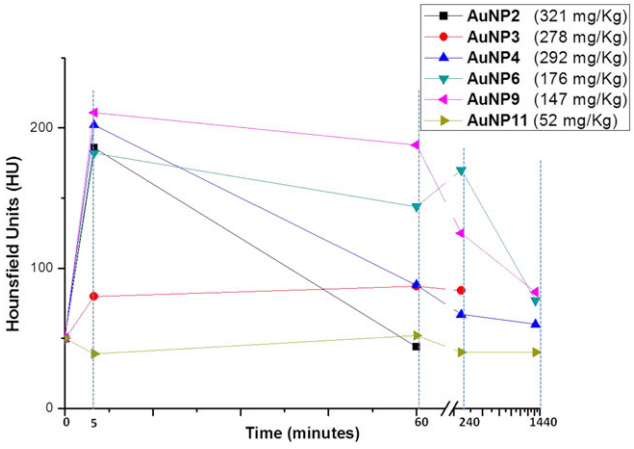

Figure 3. Trend of HU values measured within the heart as a function of the time after injection. In round brackets the dose (mg Au/Kg bw) injected via tail vein for each experiment. The HU values at 0 minutes correspond to the contrasts within the heart before injection (basal value).

significant role in CT imaging. At the same time, the anisotropic gold nanoparticles (**AuNP9**) showed a very good X-rays absorption and a prolonged persistence in the blood, paving the way to the development of innovative bimodal contrast systems.

To better delineate the *in vivo* behavior of these gold-based nano-systems, we report in Fig. 5 the distribution over time of contrast in coronal sections of three live mice, who received i.v. infusion of a different **AuNP** batch each (i.e., **AuNP3**, **AuNP6** and **AuNP9**). **AuNP3** led to an immediate increase of liver contrast, without appreciable changes in the contrast of the heart, suggesting that **AuNPs** were immediately sequestered in the liver. On the contrary, **AuNP6** and **AuNP9** led to an increase of the heart contrast at five minutes, which remained almost constant up to four hours, suggesting that **AuNPs** remained in the blood pool.

2.3. Target-functionalized gold nanoparticles

Considering the importance of developing innovative contrast agents, large efforts have been devoted to the production of nano-materials able to selectively label the region of interest, providing functional and morphological information (5,6). In this contest, having in our hands a reliable method to synthesize high quality and stable gold nanoparticles, we prepared glucosamine-functionalized spherical **AuNPs** (**AuNP7**, Scheme 1 and Table 1). Stated their *in vitro* ability to act as CT contrast agents, **AuNP7** (Fig. 6) were selected as nano-tracer for the active targeting against lung inflamed cells.

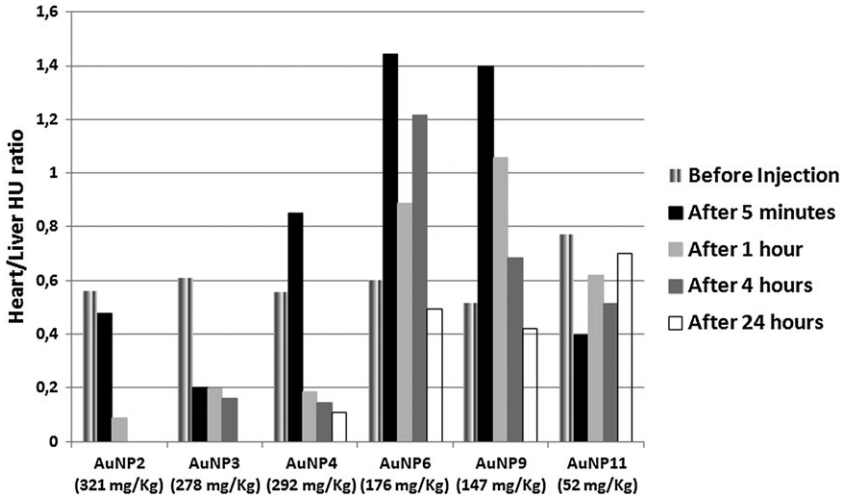

Figure 4. Heart/liver HU ratio measured 5 minutes, 1 hour, 4 hours and 24 hours after **AuNPs** injection. In the round brackets the dose amount (mg Au/Kg bw) injected for each experiment.

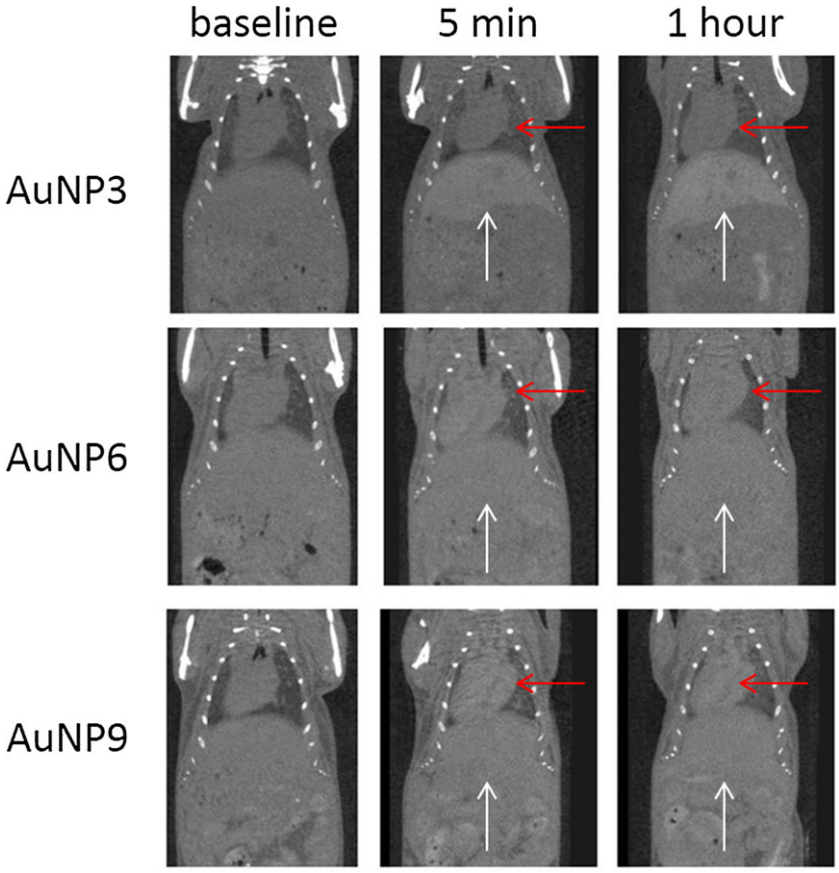

Figure 5. Coronal section of mice treated with **AuNP3**, **AuNP6** and **AuNP9**. Baseline: images obtained before infusion. White arrow: liver; red arrow: heart.

A group of 11 mice were treated with HCl, to induce a chemical pneumonia and subsequently infused with a colloidal solution of **AuNPs**. As shown in Fig. 7, the right lung (directly injured by the acid) showed inflammation and hemorrhage, while the left one did not have pathologic changes.

To evaluate *in vivo* **AuNP7** behavior, a first injured mouse received **AuNP7** colloidal solution (230 mg/Kg), showing that nanoparticles were able to selectively track the presence of lung inflammation. One hour after injection (see **SI**, Fig. 14), the presence of **AuNP7** circulating within the blood pool was demonstrated by the high contrast within the heart and by the progressive enhancement of the contrast in the lung region affected by inflammation, indicating the uptake of **AuNP7** by inflammatory cells. After 4 hours of observation, the mouse was sacrificed and lungs were removed and underwent a CT scan in order to measure the contrast *ex-vivo* in the lung (Fig. 8A).

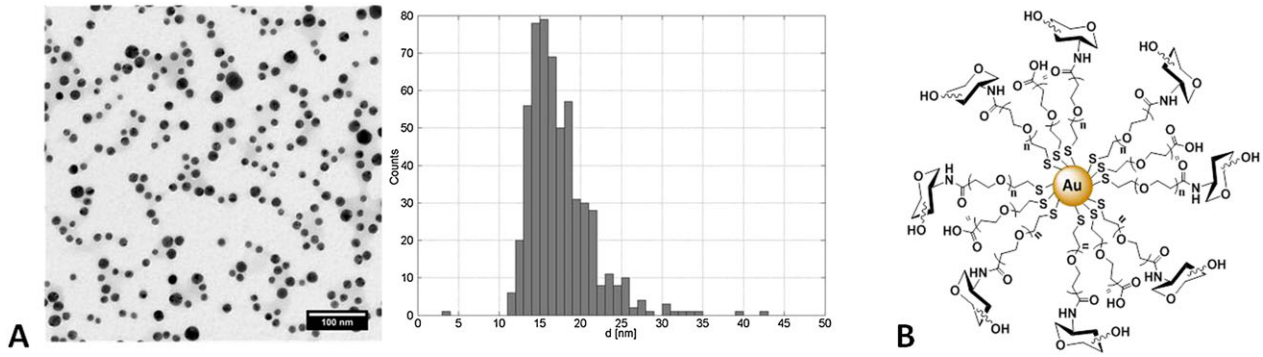

Figure 6. **AuNP7** used as functional CT contrast agents **A)** Left: TEM micrograph of **AuNP7** sample. Right: statistical distribution of particle diameters: $d_{median} = 16.6 \pm 3.9$ nm. **B)** Scheme of **AuNP7**.

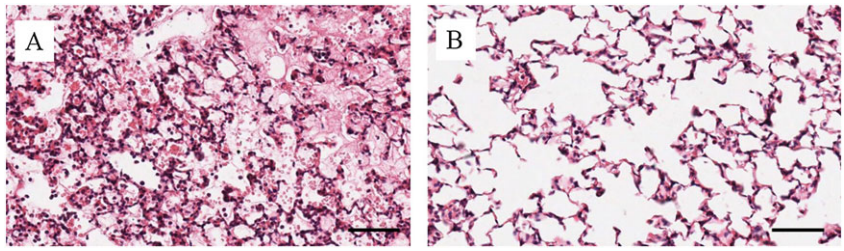

Figure 7. Representative images of hematoxylin and eosin stained lung tissue sections of acid aspiration that showed the inflammatory and serofibrinous exudate and hemorrhage in the right injured (A) lung, whereas no pathologic changes are observed in the left lung (B). (200X, scale bar = 100 μm).

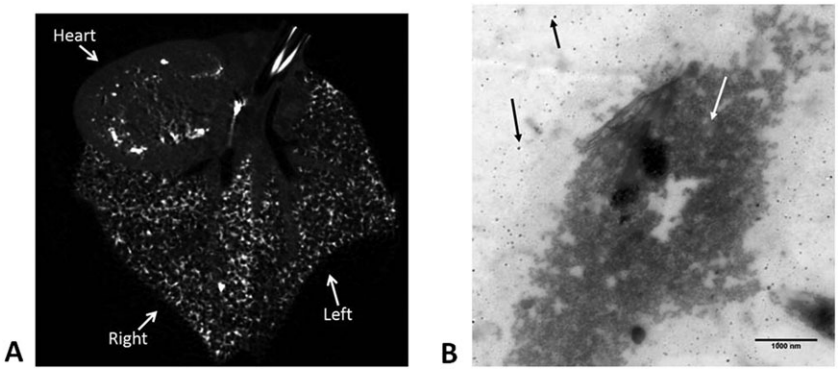

Figure 8. **A**. Computed Tomography imaging of the injured lung *ex-vivo*. The lesion at the right lung is clearly visible for its higher X-rays contrast (HU right lung = 217; HU left lung = 42). **B**. TEM images of material collected by bronchoalveolar-lavage: **AuNPs** identified by black arrow and fragment of pulmonary tissue identified by the white arrow.

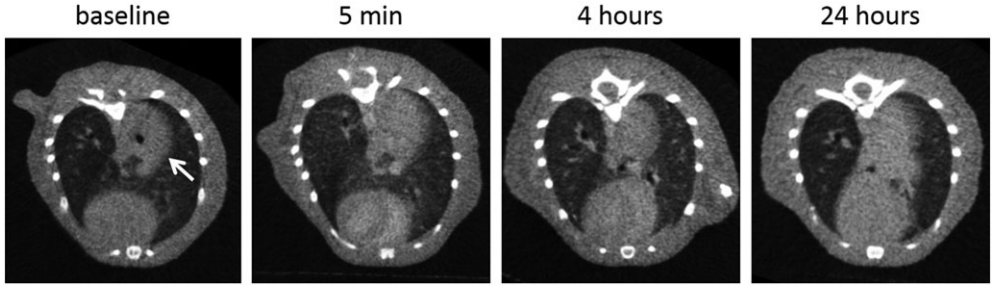

Figure 9. Transaxial sections by computed tomography obtained in live, anesthetized mice with experimental pneumonia in the dorsal region of the right lung (showed by the arrow), showing the distribution in time of **AuNP7**, after intravenous injection.

To confirm the nanoparticles presence within the cells, a bronchoalveolar lavage was performed three times in the right (injured) lung and analysed by means of electron microscopy. TEM images of the cellular samples let to show the presence of nanoparticles within fragments of lung tissue (Fig. 8B), revealing that they maintained their structure, with a median diameter of 32.5 ± 5.9 nm (32).

On the basis of these results, a new set of experiments was carried out and 10 injured mice were treated with targeted and non-targeted **AuNPs**, extending the time of animal observation up to 24 hours after injection (dose used is reported in **SI**, Tab. 1). Four mice have been treated with the control colloidal solution of **AuNP6** (coated by HS-PEG_{5000}-OMe), while six mice have been injected with targeted active **AuNP7** (coated by HS-PEG_{5000}-CONHGlucose). Owing to the displayed glucose-moiety, **AuNP7** selectively accumulated in the lung inflammation, giving both anatomical and functional image information (Fig. 9).

The **AuNP6** and **AuNP7** circulation in the blood was observed, in the whole animal group (n = 10), up to 24 hours after injection and it was possible to appreciate the increase of X-rays contrast (Fig. 10) within the heart and in the site of lesion (lung injury) (23).

Noteworthy, **AuNP7** levels in the lung injury (right lung) were higher if compared to **AuNP6**, even if this did not reach a statistically significance. In the lung lesion, the **AuNP7** remained elevated up to 24 hours after injection, which indicates their active accumulation, in contrast with the non-targeted ones. This trend was not observed in other organs. In the heart, after 5 minutes, the HU in mice treated with **AuNP7** were higher but in the following time points the two groups showed similar HU levels. The **AuNP** liver's uptake was modest in all animals, confirming the stealthness of both nano-systems. The HU increase in the bladder (observed in all animals) can be ascribed to the small fraction of ultrasmall **AuNPs**, which can be filtrated through the renal glomerulus, and highly concentrated in the small volume of the bladder (32). To confirm this interpretation, we collected urine samples after 1 hour from injection and we analysed them by TEM microscope (see SI, Fig. 15). TEM images show the presence of small **AuNPs** ($d < 5$ nm) whose numeral and dimension were compatible with **AuNP6** and **AuNP7** histograms. After 24 hours from injection, mice were sacrificed and organs (lungs and liver) were removed to quantify the amount of gold accumulated within each. The removed organs were then digested with *aqua regia* and the amount of metal in each organ was measured by means of ICP-OES analysis. The results, reported in Fig. 11, are consistent with the CT trend. The metal accumulation in the lung injury (right lung) was higher for mice treated with **AuNP7** as compared to those treated with the non-targeted ones (**AuNP6**). Left lungs, instead, show a similar amount of gold both for mice injected with **AuNP6** as with **AuNP7**, highlighting how the glucosamine-functionalized nanoparticles were selective towards the site of inflammation.

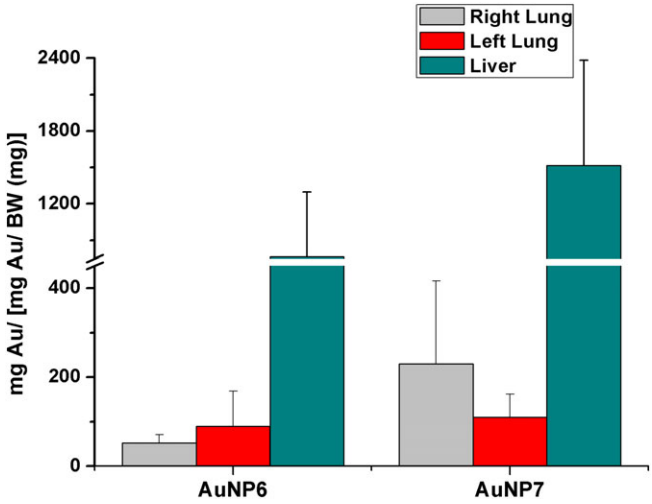

Figure 11. ICP-OES analysis of liver and lungs of sacrificed mice after 24 hours from injection of **AuNP6** (n = 4) and **AuNP7** (n = 6). The abscissa reports the amount of gold found in the organ (mg) normalized for the dose injected to each mouse (mg Au/mg BW).

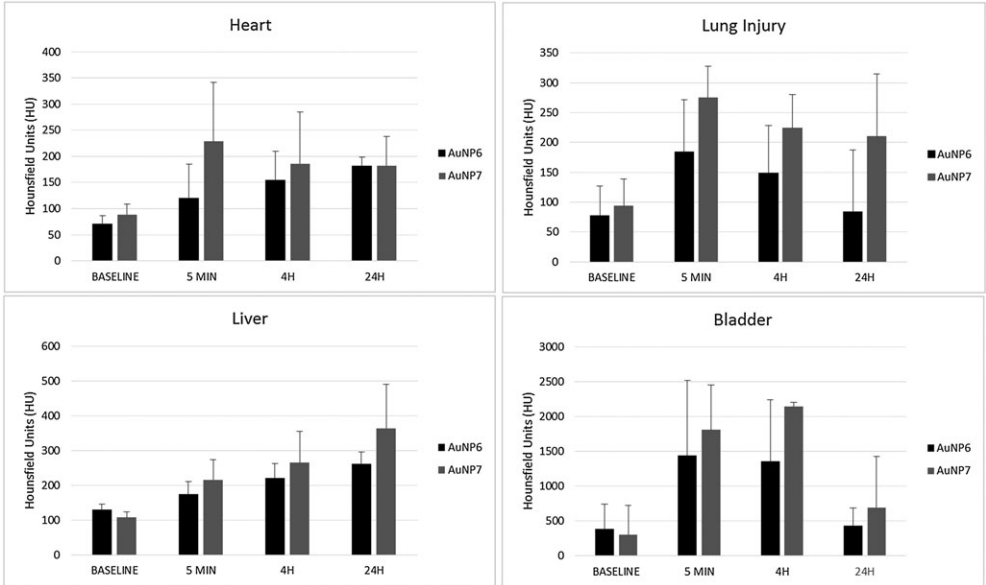

Figure 10. **AuNP6** (n = 4) and **AuNP7** (n = 6) contrast values measured within the heart, lung injury, liver and bladder at different time points after injection.

3. CONCLUSIONS

In this work, we have been able to identify the nano-structures which better respond to the requisite for acting as a good pre-clinical contrast nano-agents. We presented a modified protocol for the 'one-pot' production of functionalized shape-controlled nanoparticles (from symmetric to anisotropic shapes). Our protocols allowed to obtain reproducible and highly stable engineered nanoparticles. **AuNP6**, **AuNP7** and **AuNP9** proved to be excellent candidates as CT contrast agents, having an increased blood-time permanence and a low uptake from the reticuloendothelial system (RES). Nevertheless, no significant differences were found when using anisotropic nanoparticles as opposed to symmetric ones. Noteworthy, stable glucosamine-functionalized **AuNPs** (**AuNP7**) proved to act as efficient contrast agents targeted towards glucose uptake as they accumulated preferentially in the lung injured by chemical pneumonia in mice, *in vivo*. Further studies are currently undergoing to evaluate organ toxicity and to better describe the internalization of the gold nanoparticles in the cells and how the uptake of glucosamine-functionalized particles reflects the actual cellular glycolytic metabolism.

4. MATERIALS AND METHODS

4.1. Materials

All reagents were purchased from Sigma-Aldrich, unless mentioned otherwise, and used without further purification. $HAuCl_4 \cdot 3H_2O$ was stored at 4 °C in the dark as 10 mM solution. $AgNO_3$ solution (5.9 mM) was freshly prepared before each synthesis (avoiding the exposition to the light). HS-PEG_{5000}-CH_3O and HS-PEG_{5000}-COOH, purchased from Rapp Polymer GmbH, were used as received and stored under dry argon atmosphere at −20 °C. All glassware used for **AuNPs** synthesis was cleaned with *aqua regia* (HCl(37%) / HNO_3(65%) 3/1). Ultrapure deionized water, MilliQ water, was used for the preparation of aqueous solutions. Purification of **AuNPs** was performed by ultrafiltration using Millipore Amicon Ultra-4 Centrifugal Filter Units with a cut-off of 30 KDa. **AuNPs** were characterized by Dynamic Light Scattering (DLS), using a 90 Plus Particle Size Analyzer from Brookhaven Instrument Corporation (Holtsville, NY, USA) operating at 15 mW of a solid-state laser ($\lambda = 661$ nm), using a scattering angle of 90 °C. The Zeta-potential was determined at 25 °C using a 90 Plus Particle Size Analyzer from Brookhaven Instrument Corporation (Holtsville, NY, USA) equipped with an AQ-809 electrode, operating at applied voltage of 120 V. UV/Vis spectra were recorded on an Agilent 8453 instrument (Agilent Technologies, Santa Clara, CA, USA). A disposable cuvette with 1 cm optical path length was used for the measurements. FTIR spectra were recorded using Thermo Nicolet NEXUS 670 FTIR spectrometer. The samples were prepared as KBr pellets by titration with KBr powder (1:100). Transmission Electron Microscopy micrographs have been collected using TEM-Zeiss LIBRA 200FE, equipped with: 200 kV FEG, in column second-generation omega filter for energy selective spectroscopy (EELS) and imaging (ESI), HAADF STEM facility, EDS probe for chemical analysis, integrated tomographic HW and SW system). The concentration of gold was determined via Inductively Coupled Plasma-Optical Emission Spectrometers (ICP-OES; iCAP 6300 Duo, Thermofisher). High resolution MALDI were performed at CIGA (Centro Interdipartimentale Grandi Apparecchiature, Milan, Italy), by means of MALDI tof-tof Autoflex II instrument.

4.2. Synthesis of functionalized AuNPs

4.2.1. Synthesis of AuNP2, AuNP3 and AuNP4

A water solution of sodium citrate (3 mL, 68 mM), $HAuCl_4 \cdot 3H_2O$ (2.5 ml, 10 mM) and $AgNO_3$ (140 μl, 5.9 mM) were prepared and stirred at room temperature for 6 min. The pre-incubated mixture was, then, added to a 500 mL flask containing 250 mL of boiling water. The mixture stirred (750 rpm) for 1 h at 100 °C, then the seeds solution was allowed to cool to room temperature. A second mixture of sodium citrate (16.5 mL, 34 mM), $HAuCl_4$ (12.5 mL, 10 mM) and $AgNO_3$ (600 μL, 5.9 mM) was pre-incubated for 6 min and afterwards added to the seeds solution, followed immediately by the addition of a solution of hydroquinone (13.3 mL, 91 mM). Then, the solution was allowed to age, stirring at 750 rpm for 1 h. **AuNP1** so obtained was directly used without further purification or concentration. Under argon atmosphere, 30 mg of the suitable thio-PEG [HOOC-PEG_{5000}-SH (**AuNP2**) or 1:1 mixture of HOOC-PEG_{5000}-SH/MeO-PEG_{5000}-SH (**AuNP3**) or MeO-$PEG5_{000}$-SH (**AuNP4**) were dissolved in 5 mL of water containing 9 mg of NaOH. Then, the PEG solution was added to the mixture containing citrate-capped **AuNP1** while Argon was bubbling inside the solution (for 5 minutes) and the reaction mixture stirred for further 48 h at room temperature. Functionalized **AuNP2-4** were then concentrated and purified by means of Amicon centrifugal Filter units to a final volume of 700 μL.

4.2.2. Synthesis of AuNP6 and AuNP7

A solution of sodium citrate (9 mL, 68 mM), $HAuCl_4$ (7.5 ml, 10 mM) and $AgNO_3$ (490 μL, 5.9 mM) were prepared and stirred at room temperature for 6 min. The pre-incubated mixture was, then, added to a 500 mL flask containing 250 mL of boiling water. After 1 h of mixing at 100 °C (750 rpm) the seeds solution was allowed to cool at room temperature and 5 mL of glycerol was added. After 10 min a second mixture of sodium citrate (10 mL, 34 mM), $HAuCl_4$ (7.5 mL, 10 mM) and $AgNO_3$ (426 μL, 5.9 mM), pre-mixed for 6 min, was added to the seeds solution, immediately followed by a solution of hydroquinone (8 mL, 91 mM). Then, the solution was allowed to age, stirring at 750 rpm for 1 h. **AuNP5** so obtained was directly used without further purification or concentration. Under argon atmosphere, 30 mg of the suitable thio-PEG [MeO-PEG_{5000}-SH (**AuNP6**) or HS-PEG_{5000}CONHGlucose (see **SI**, **AuNP7**)] were dissolved in 5 mL of water containing 9 mg of NaOH. Then, the PEG solution was added to the colloidal solution containing citrate-capped **AuNP5** while Argon was bubbling inside the solution (for 5 minutes) and the reaction mixture stirred for further 48 h at room temperature. Functionalized **AuNP6** and **AuNP7** were then concentrated and purified by means of Amicon centrifugal Filter units to a volume of 700 μL.

4.2.3. Synthesis of AuNP9

A solution of sodium citrate (1.73 mL, 68 mM), $HAuCl_4$ (1.46 mL, 10 mM) and $AgNO_3$ (82 μL, 5.9 mM) were prepared and mixed at room temperature for 6 min. The pre-incubated mixture was, then, added to a 1000 mL flask containing 60 mL of boiling water. After 1 h of mixing at 100 °C (750 rpm) the solution was

cooled at room temperature and 54 mL of glycerol and 600 mL of water were added. After 10 min a second mixture of sodium citrate (1.16 mL, 34 mM), $HAuCl_4$ (13.4 mL, 10 mM) and $AgNO_3$ (2.2 mL, 5.9 mM) pre-mixed for 6 min, was added to the seeds solution, immediately followed by a solution of hydroquinone (5.3 mL, 91 mM). Then, the solution was allowed to age, stirring at 750 rpm for 1 h. The bluish solution of **AuNP8** was directly used without further purification or concentration. Under argon atmosphere, 30 mg of MeO-PEG_{5000}-SH were dissolved in 5 mL of water containing 9 mg of NaOH. Then, the PEG solution was added to citrate-capped **AuNP8** solution while Argon was bubbling inside the solution (for 5 minutes) and the reaction mixture stirred for further 48 h at room temperature. Functionalized **AuNP9** were then concentrated and purified by means of Amicon centrifugal Filter units to a volume of 700 μL.

4.2.4. *Synthesis of AuNP11 (31)*

A solution of tetrachloroauric acid (7.5 mL, 10 mM) was diluted with 200 mL of water. Next, 6 mL of an aqueous hydroquinone solution (11 mg mL^{-1}) was rapidly injected. The solution turned from yellow to light blue almost instantaneously because of the formation of gold nanostars. 30 mg of MeO-PEG_{5000}-SH was added to the mixture to quench the reaction and cap the **AuNPs**. Functionalized **AuNP11** were then concentrated and purified by means of Amicon centrifugal Filter units to a volume of 700 μL.

4.3. AuNPs characterization

The purification and concentration of **AuNPs** were performed by centrifugation at 6000 rpm on filters with a cut-off of 30 KDa. The solutions were filtered over 0.45 μm minisart. Then the concentration of the colloidal solution was completed, in Eppendorf tubes at 14000 rpm, up to 700 μL. TEM specimens were prepared by dropping an aqueous solution of **AuNPs** onto on a carbon-coated copper grid (300 mesh) and evaporating the solvent. The particle size distribution, in the spherical and quasi spherical samples, was obtained analysing TEM images by the software Pebbles (freely available from the http://pebbles.istm.cnr.it) (33). Dimensions of star-shape nanoparticles have been estimated by measuring the distance between diametrically opposite branches using ITEM-TEM Imaging platform – Olympus Soft Imaging Solutions. The number of measured nanoparticles for each sample is around 250. UV/Vis spectra were recorded on an Agilent 8453 instrument. DLS and ζ-potential measurements were carried out on a Brookhaven 90 PLUS particles size analyser. DLS samples were prepared by filtration with a 0.45 μm cellulose acetate syringe filter before loading into the cuvette in order to remove large interfering particulate matter. Each sample was allowed to equilibrate for 3 min prior to starting measurement. Three to 10 independent measurements of 60 s duration were performed, at 25 °C. The hydrodynamic diameter calculations were performed using Mie theory, considering absolute viscosity and refractive index values of the medium to be 0.911 cP and 1.334, respectively. The Zeta-potential was automatically calculated from electrophoretic mobility based on the Smoluchowski theory. A viscosity of 0.891 cP, a dielectric constant of 78.6, and Henry function of 1.5 were used for the calculations. FTIR spectra samples were prepared as KBr pellets by titration with KBr powder (1:100). The content of the metal was determined by ICP-OES. Samples (1 ml each) were digested in a glass vial over a heating plate with *aqua regia* (2 mL) for four times. The dry residuals were dissolved in an HCl aqueous solution 0.5 M and properly diluted. The limit of detection (lod) calculated for gold was 0.01 ppm.

4.4. *In vivo* CT analysis

CD1 mice (20–25 g) were obtained from Harlan Laboratories (Udine, Italy) and kept under laboratory condition. Procedures involving animals and their care were performed according to the institutional guidelines which complied with national and international laws and policies. The study was approved by the ethical committee of our institution. We studied two sets of animals, healthy (**AuNP 3-4-6-9-11**) and injured (**AuNP6** and **AuNP7**). The first set was aimed at screening and characterizing **AuNPs** and one animal for each type of nanoparticle was used. After the selection of the most appropriate **AuNPs**, the experiments were repeated in four mice for **AuNP6** and 6 mice for **AuNP7**. Animals were anesthetized by using ketamine and xilazine. Lung injury was induced by instillation of 1.5 mL/kg HCl 0.1 M into the right bronchus through a small tracheal incision (34). The bronchial catheter was removed and the tracheal incision sutured. Animals were awakened and **AuNPs** injection and imaging were performed 24 hours later to allow the development of the inflammatory reaction. For imaging healthy and injured anesthetized mice received PEG-capped AuNPs (Au concentration depended on the batches, see to Table 1, 200 μL) injected via tail vein (i.v.) and underwent CT scans (Skyscan 1176, Bruker, Kontich, Belgium) at different time points (immediately before [baseline], five minutes, one and four hours after injection). CT scanning lasted for about five minutes (voltage 58 kV, current 431 μA). Images were reconstructed with a smoothing filter and corrected for ring artifact and beam hardening. Reconstructed isotropic voxel size was 35 μm^3. Images were reconstructed and analysed with the scanner software (NRecon v.1.6.9 and CTAn v.1.13, Skyscan, Bruker, Kontich, Belgium). For image analysis, we firstly calibrated Hounsfield Units (HU) scale, by scanning a phantom made of air and water, by ascribing the values 0 HU to water and −1000 HU to air. We then measured, at all time points, the density (in HU) on manually selected Regions of Interest (ROIs) on the heart, liver and on the injured lung.

Sample preparation of bronchoalveolar lavage: 600 μL of lavage solution and cells were collected from right lung and fixed in 2.5% glutaraldehyde and 4% paraformaldehyde. This collected material was centrifuged and the resulted pellet was suspended in equal volume of sodium alginate solution. Drops of this cells/alginate suspension of 15 μL were drown into a Eppendorf-type micro-pipette and extruded firmly into a buffer containing 0.1 M calcium chloride pH 7.2. These drops were included in Epoxy/Araldite resin, then the series of section were prepared for the TEM analysis. For histologic examination, lungs were fixed in 4% paraformaldehyde, then paraffin embedded and stained with hematoxylin and eosin. The metal content in lungs and livers was determined by ICP-OES. Samples of homogenized organs in PBS solutions (1 mL each) were digested in a glass vial over a heating plate with *aqua regia* (2 mL) for 10 times. The dry residuals were dissolved in a HCl aqueous solution 0.5 M and properly diluted. The limit of detection (lod) calculated for gold was 0.01 ppm.

Acknowledgements

A.S., L.P. and A.M.F. thank 'RSPPTECH-Convenzione Operativa inserita nella Raccolta Convenzioni e Contratti della Regione Lombardia (grant number 18095/RU)'. L.P. thanks MIUR-Italy (PRIN 2010–2011: contract 2010JMAZML_003).

REFERENCES

1. Schmidt CW. CT scans: Balancing health risks and medical benefits. Environ Health Perspect 2012; 120(3): a118–a121.
2. Schenkman L. Second thoughts about CT imaging. science 2011; 331: 1002–1004.
3. Jin E, Lu Z-R. Biodegradable iodinated polydisulfides as contrast agents for CT Angiography. Biomaterials 2014; 35: 5822–5829.
4. Hallouard F, Anton N, Choquet P, Constantinesco A, Vandamme T. Iodinated blood pool contrast media for preclinical X-ray imaging applications – a review. Biomaterials 2010; 31: 6249–6268.
5. Lee N, Choi SH, Hyeon T. Nano-sized CT contrast agents. Adv Mater 2013; 25: 2641–2660.
6. Jakhmola A, Anton N, Vandamme TF. Inorganic nanoparticles based contrast agents for x-ray computed tomography. Adv Healthcare Mater 2012; 1: 413–431.
7. Trono JD, Mizuno K, Yusa N, Matsukawa T, Yokoyama K, Uesaka M. Size, concentration and incubation time dependence of gold nanoparticle uptake into pancreas cancer cells and its future application to x-ray drug delivery system. J Radiat Res 2011; 52: 103–109.
8. Ahn S, Jung SY, Lee SJ. Gold nanoparticle contrast agents in advanced x-ray imaging technologies. Molecules 2013; 18: 5858–5890.
9. Ng VWK, Berti R, Lesage F, Kakkar A. Gold: a versatile tool for *in vivo* imaging. J Mater Chem B 2013; 1: 9–25.
10. Kim JY, Ryu JH, Schellingerhout D, Sun IC, Lee SK, Jeon S, Kim J, Kwon IC, Nahrendorf M, Ahn CH, Kim K, Kim DE. Direct imaging of cerebral thromboemboli using computed tomography and fibrin-targeted gold nanoparticles. theranostics 2015; 5(10): 1098–1114.
11. Domey J, Teichgräber U, Hilger I. Gold nanoparticles allow detection of early-stage edema in mice via computed tomography imaging. Int J Nanomedicine 2015; 10: 3803–3814.
12. Cole LE, Vargo-Gogola T, Roeder RK. Contrast-enhanced x-ray detection of Microcalcifications in Radiographically Dense Mammary Tissue Using Targeted Gold nanoparticles. ACSNano 2015; 9(9): 8923–8932.
13. Wang Z, Wu L, Cai W. Size-tunable synthesis of monodisperse water-soluble gold nanoparticles with high x-ray attenuation. Chem Eur J 2010; 16: 1459–1463.
14. Silvestri A, Polito L, Bellani G, Zambelli V, Jumde RP, Psaro R, Evangelisti C. Gold nanoparticles obtained by aqueous digestive ripening: Their application as X-ray contrast agents. J Colloid Interface Sci 2015; 439: 28–33.
15. Nehl CL, Liao H, Hafner JH. Optical properties of star-shaped gold nanoparticles. Nano Lett 2006; 6(4): 683–688.
16. Yuan H, Fales AM, Vo-Dinh T. TAT peptide-functionalized gold nanostars: enhanced intracellular delivery and efficient NIR photothermal therapy using ultralow irradiance. J Am Chem Soc 2012; 134: 11358–11361.
17. Li N, Zhao P, Astruc D. Anisotropic gold nanoparticles: synthesis, properties, applications, and toxicity. Angew Chem Int Ed 2014; 53: 1756–1789.
18. Assanhou AG, Alolga RN, Onoja V, Agbokponto JE, Kassim SA, Sabi-mouka EMB. Polymers used for surface modifications in stealth liposomes preparations: a review. World J Pharmaceut Res 2015; 4(4): 2064–2086.
19. Warburg O. The metabolism of tumors. Constable and Co.: London, 1930.
20. Alexander E. Glioblastoma revisited: do clinical observations match basic science theory? Radiosurgery: clinical observations. J Neurooncol 1993; 15: 169–173.
21. Urakami K, Zangiacomi V, Yamaguchi K, Kusuhara M. Impact of 2-deoxy-D-glucose on the target metabolome profile of a human endometrial cancer cell line. Biomed Res 2013; 34(5): 221–229.
22. Gambhir SS. Molecular imaging of cancer with positron emission tomography. Nat Rev Cancer 2002; 2: 683–693.
23. Zambelli V, Di Grigoli G, Scanziani M, Valtorta S, Amigoni M, Belloli S, Messa C, Pesenti A, Fazio F, Bellani G, Moresco RM. Time course of metabolic activity and cellular infiltration in a murine model of acid-induced lung injury. Intensive Care Med 2012; 38: 694–701.
24. Boisselier E, Astruc D. Gold nanoparticles in nanomedicine: preparations, imaging, diagnostics, therapies and toxicity. Chem Soc Rev 2009; 38: 1759–1782.
25. Jimenez-Ruiz A, Perez-Tejeda P, Grueso E, Castillo PM, Prado-Gotor R. Nonfunctionalized gold nanoparticles: synthetic routes and synthesis condition dependence. Chem Eur J 2015; 21: 9596–9609.
26. Fry HF, Hamiltox GA, Turkevich J. The kinetics and mechanism of hydrolysis of tetrachloroaurate(III). Inorg Chem 1966; 5(11): 1943–1946.
27. Zhao P, Li N, Astruc D. State of the art in gold nanoparticle synthesis. Coord Chem Rev 2013; 257: 638–665.
28. Schutz M, Steinigeweg D, Salehi M, Kompeb K, Schlucker S. Hydrophilically stabilized gold nanostars as SERS labels for tissue imaging of the tumor suppressor p63 by immuno-SERS microscopy. Chem Commun 2011; 47: 4216–4218.
29. Karakoti AS, Das S, Thevuthasan S, Seal S. PEGylated inorganic nanoparticles. Angew Chem Int Ed 2011; 50: 1980–1994.
30. Terkaya IN, Budanov VV, Ermolina LV. Preparation of stable copper dispersion by redox reactions of Cu(II) salts with sulfur-containing reducing agents and properties of the dispersions. Russ J Appl Chem 2003; 76(6): 871–874.
31. Morasso C, Mehna D, Vanna R, Bedoni M, Forvi E, Colombo M, Prosperi D, Gramatica F. One-step synthesis of star-like gold nanoparticles for surface enhanced Raman spectroscopy. Mater Chem Phys 2014; 143: 1215–1221.
32. Perez-Campana C, Gomez-Vallejo V, Puigivila M, Martin A, Calvo-Fernandez T, Moya SE, Ziolo RF, Reese T, Llop J. Biodistribution of different sized nanoparticles assessed by positron emission tomography: a general strategy for direct activation of metal oxide particles. ACS Nano 2013; 7: 3498–3505.
33. Mondini S, Ferretti AM, Puglisi A, Ponti A. PEBBLES and PEBBLEJUGGLER: software for accurate, unbiased, and fast measurement and analysis of nanoparticle morphology from transmission electron microscopy (TEM) micrographs. Nanoscale 2012; 4: 5356–5372.
34. Amigoni M, Bellani G, Scanziani M, Masson S, Bertoli E, Radaelli E, Patroniti N, Di Lelio A, Pesenti A, Latini R. Lung injury and recovery in a murine model of unilateral acid aspiration. Anesthesiology 2008; 108: 1037–1046.

SUPPORTING INFORMATION

Additional supporting information can be found in the online version of this article at the publisher's website.